ELSEVIER

18 May 1998

PHYSICS LETTERS A

Physics Letters A 242 (1998) 83–93

Two pitchfork bifurcations in the polar quadratic Zeeman–Stark effect

José P. Salas [a], A. Deprit [b], Sebastián Ferrer [c], Víctor Lanchares [d], Jesús Palacián [e]

[a] *Area de Física Aplicada, Universidad de La Rioja, 26004 Logroño, Spain*
[b] *National Institute of Standards and Technology, Gaithersburg, MD 20899-1000, USA*
[c] *Departamento de Matemática Aplicada, Universidad de Murcia, 30203 Cartagena, Spain*
[d] *Departamento de Matemáticas y Computación, Universidad de La Rioja, 26004 Logroño, Spain*
[e] *Departamento de Matemática e Informática, Universidad Pública de Navarra, 31006 Pamplona, Spain*

Received 20 January 1998; accepted for publication 4 February 1998
Communicated by V.M. Agranovich

Abstract

In the framework of classical mechanics, a study of the hydrogen atom in the presence of parallel electric and magnetic fields is presented when the magnetic quantum number m is zero. By means of perturbation methods and Poincaré surfaces of section, the existence of the three states experimentally detected by Cacciani et al. (the so-called I, II, and III Cacciani's states), their energy extensions, their evolution and their disappearance are explained as a result of two pitchfork bifurcations.

PACS: 32.60.+i; 03.65.Sq; 02.90.+p
Keywords: Zeeman effect; Stark effect; Equilibria; Bifurcation; Periodic orbits

1. Introduction

During the last years, an increasing and renewed interest in the classical dynamics of Rydberg atoms in the presence of parallel electric and magnetic fields (the so-called SQZE problem) has led to a plethora of experimental and theoretical works related to this subject. For a review of the problem, we refer the reader to the works of Waterland et al. [1], Cacciani et al. [2–4], Farrelly et al. [5], Deprit et al. [6] and Milczewski and Uzer [7].

In the same spirit as our previous work on this problem when the magnetic quantum number m is not zero [6], the aim of this Letter is to complete that study considering the special case of $m = 0$: the polar case. Thus, it is our task to establish on both analytical and numerical grounds the classical dynamics in the polar SQZE problem. As for the case m not equal zero, we consider the electric and magnetic interactions to be weak compared to the Coulomb one, in such a way that the problem is amenable analytically by classical perturbation methods. Beside this perturbation treatment, we use the numerical method of the Poincaré surfaces of section [8] which permits one to find the classical phase space structure of this problem. The application of the Poincaré surfaces of section to the case m not equal zero is now in progress.

The Letter is organized as follows. Section 2 is devoted to the posing of the problem. In Section 3, after a Delaunay normalization, a classical perturbative

PII S0375-9601(98)00116-9

study of the truncated normalized Hamiltonian system is made. This study involves the analysis of the stability of the equilibrium points, their bifurcations and the phase flow evolution. The phase flow is related with the experimental and semiclassical investigations of the Stark structure of the diamagnetic manifold of lithium carried out by Cacciani et al. [2–4]. In Section 4, by means of Poincaré surfaces of section, the transition from the Zeeman to the Stark effect is explored intensively for different values of the field strengths. Again, special attention is paid to the stability and bifurcations of the fixed points appearing in the surfaces of section, and the relation with the investigations of Cacciani et al.

2. The problem

Let us consider the motion of an electron of mass μ and charge f in a Coulomb field induced by a infinitely massive nucleus of charge $e > 0$ at rest. On the central field are superimposed a uniform constant magnetic field $\boldsymbol{B}$ and a uniform constant electric field $\boldsymbol{f}$. The fields are parallel, that is to say, there exists a unit vector $\boldsymbol{k}$ fixed in space such that

$$\boldsymbol{B} = B\boldsymbol{k}, \quad \boldsymbol{f} = f\boldsymbol{k},$$

the strengths B and f being uniformly constant and positive.

Denoting by $\boldsymbol{r}$ the position of the electron with respect to the center of the Coulomb field, and adopting atomic units ($\mu = e = 1$), we find that the Hamiltonian of the system is

$$\mathcal{H} = \tfrac{1}{2}||\boldsymbol{P} - \omega(\boldsymbol{k} \times \boldsymbol{r})||^2 - \frac{1}{||\boldsymbol{r}||} + f(\boldsymbol{k} \cdot \boldsymbol{r}), \qquad (1)$$

where $\omega = B/2$ is the Larmor frequency corresponding to the field $\boldsymbol{B}$. For more details see Ref. [6].

Clearly, the system defined by the Hamiltonian (1) is invariant for rotations about the axis $\boldsymbol{k}$ of the electric and magnetic fields. Accordingly, $m = \boldsymbol{k} \cdot (\boldsymbol{r} \times \boldsymbol{P})$, that is, the projection of the total angular momentum of the particle on the field lines, is an integral.

A canonical transformation that is time dependent allows us to formulate the problem in a frame of reference rotating with angular velocity ω. In the moving frame, the Larmor precession is removed at order one, and the Hamiltonian describing the system becomes

$$\mathcal{H} = \tfrac{1}{2}||\boldsymbol{P}||^2 - \frac{1}{||\boldsymbol{r}||} + \frac{\omega^2}{2}||\boldsymbol{k} \times \boldsymbol{r}||^2 + f(\boldsymbol{k} \cdot \boldsymbol{r}). \qquad (2)$$

In cylindrical coordinates ($\rho, z, \phi, P_\rho, P_z, P_\phi = m$), the Hamiltonian (2) becomes

$$\mathcal{H} = \frac{1}{2}\left(P_\rho^2 + P_z^2 + \frac{m^2}{2\rho^2}\right)\frac{1}{\sqrt{\rho^2 + z^2}} + \frac{\omega^2}{2}\rho^2 + fz, \qquad (3)$$

where we observe that the Hamiltonian (3) defines a dynamical system of two degrees of freedom, depending on the three parameters m, f and ω. Throughout, we restrict ourselves to the manifold $m = 0$. In that case, the problem depends on the two parameters f and ω.

As we will see, it is convenient to introduce a frequency σ and a rheostat parameter λ in the interval $[0, 1]$ such that

$$\omega = 4\sigma^2\lambda, \quad f = \sigma^2 a(\lambda - 1). \qquad (4)$$

If $\lambda = 0$ then $\omega = 0$, which means that the perturbation is caused exclusively by the Stark effect; furthermore, if $\lambda = 1$ then $f = 0$ and the perturbation consists exclusively of the Zeeman effect. In other words, λ controls the respective mix of the Zeeman and Stark effects.

3. Classical perturbative study

3.1. The normalized Hamiltonian

The Hamiltonian (3) may conveniently be split into the sum $\mathcal{H} = \mathcal{H}_0 + \mathcal{H}_1$ with

$$\mathcal{H}_0 = \tfrac{1}{2}(P_\rho^2 + P_z^2) - \frac{1}{\sqrt{\rho^2 + z^2}},$$

$$\mathcal{H}_1 = 2\omega^2\rho^2 + fz, \qquad (5)$$

where the term $\mathcal{H}_0$ stands for a pure Keplerian system, while the term $\mathcal{H}_1$ describes the presence of the two external fields.

For bounded orbits, $\mathcal{H}_0 < 0$, to each negative value of $\mathcal{H}_0$ corresponds a frequency n and a length a which are, respectively, the frequency and semi-major axis of the Keplerian orbits. Following the Solove'v perspective [6,9,10], we assume that $\omega \ll n$ and $f \approx a\omega^2$. Under these conditions, the Hamiltonian $\mathcal{H}_1$ can be

treated as a first order perturbation of the Hamiltonian $\mathcal{H}_0$.

Following the literature on the subject [1,6,11,12], we perform the normalization in the Delaunay variables[1] $(I_2, I_3, \phi_2, \phi_3)$. The so-called Delaunay normalization [14] is a canonical transformation,

$$(I_2, I_3, \phi_2, \phi_3) \to (I_2', I_3', \phi_2', \phi_3')$$

that converts the function $\mathcal{H}$ into a series expansion that, truncated, does not depend on the averaged mean anomaly ϕ_3'. We find that we do not need to carry out the operation beyond the first order; therefore, neglecting additional terms of higher order, we get $\mathcal{H}'$ simply by averaging the function $\mathcal{H}$ in Eq. (2) over the mean anomaly ϕ_3. With these conventions the normalized Hamiltonian comes out as the sum $\mathcal{H}' = \mathcal{H}_0' + \mathcal{H}_1'$.

As ϕ_3' is negligible in $\mathcal{H}'$, its conjugate moment I_3' is an integral, thus $\mathcal{H}_0'$ may be neglected and the normalized Hamiltonian is reduced to

$$\mathcal{H}' \equiv \mathcal{H}_1' = \tfrac{1}{2}\sigma^2 a^2 \{ \tfrac{1}{2}[(1 + \tfrac{3}{2}e^2) + \tfrac{5}{2}e^2 \cos 2\phi_2]\lambda - 3e(1-\lambda)\sin\phi_2 \}, \quad (6)$$

where $e = \sqrt{1 - I_2^2/I_3^2}$ is the eccentricity of the Keplerian orbits. For convenience, we will drop the primes on the normalized variables. We do not enter into the details of the algebraic operations involved in constructing the normalized Hamiltonian. They were executed with the symbolic processor Mathematica [15].

In this way, the Hamiltonian function (6) defines a one degree of freedom system. It remains with this integrable system to understand the role played by the parameters (the relative strength of the electric and magnetic fields) in the structure of the flow when those parameters change.

3.2. *Phase flow on the sphere and equilibrium points*

It is worth noticing that the maps of $\mathcal{H}'$ on the cylinders (ϕ_2, I_2) do not cover the entire phase space, because they exclude the points $e = 0$ (circular orbits) at which the argument of perinucleus ϕ_2 is not defined. This singularity, as Deprit and Ferrer show [16], disappears when the system is handled in the following variables,

$$u = e\cos\phi_2, \quad v = e\sin\phi_2,$$
$$w = \pm\sqrt{1-e^2} = \pm\frac{I_2}{I_3}, \quad (7)$$

where we recognize the Cartesian components of the Runge–Lenz vector A, and the norm of the angular momentum I_2 divided by I_3. In this new map (u, v, w), since

$$S \equiv u^2 + v^2 + w^2 = 1,$$

the phase space consists of a unit radius sphere S. In these coordinates, the points with $w > 0$ $(I_2 > 0)$ stand for Keplerian ellipses traveling in a direct (prograde) sense, while points with $w < 0$ $(I_2 < 0)$ represent Keplerian ellipses traveling in a retrograde sense. Moreover, any point in the equatorial circle $w = 0$ $(I_2 = 0)$ corresponds to a straight line passing through the origin. Finally, the north (south) pole corresponds to circular orbits $(e = 0)$ traveled in a direct (retrograde) sense.

In coordinates (u, v, w) the Hamiltonian $\mathcal{H}'$ becomes the function

$$\mathcal{H}' = \tfrac{1}{2}\sigma^2 a^2 [\tfrac{1}{2}(1 + 4u^2 - v^2)\lambda - 3v(1-\lambda)]. \quad (8)$$

Taking into account the Liouville–Jacobi theorem and the Poisson brackets between the variables (u, v, w),

$$[u, v] = w, \quad [v, w] = u, \quad [w, u] = v,$$

the equations of motion associated with $\mathcal{H}'$ are

$$\dot{u} = (u; \mathcal{H}') = [3(\lambda - 1) - \lambda v]w,$$
$$\dot{v} = (v; \mathcal{H}') = -4\lambda u w,$$
$$\dot{w} = (w; \mathcal{H}') = [-3(\lambda - 1) + 5\lambda v]u. \quad (9)$$

The topology of the phase flow is determined for the most part by the equilibria and their stability. The equilibria of the system are the local extrema of $\mathcal{H}'$ on S. They are the roots of the system made of the right hand members of Eq. (9) equated to 0 together with the relation S. The above equations have the symmetry

$$(u, t) \to (-u, -t), \quad (w, t) \to (-w, -t),$$

which indicates that the phase flow is time reversal symmetric with respect to the planes $u = 0$ and $w = 0$. Consequently, equilibria, if any, must lie in the plane $u = 0$ and (or) in the plane $w = 0$.

[1] For a definition, see Ref. [13]; notations adopted in this Letter are those of Ref. [12].

Table 1
Conditions of existence, energy and kind of orbit of the equilibria. The labels parallel and perpendicular indicate the position of the periodic orbit with respect to the direction of the external fields

Equilibrium	Existence	Energy	Kind of orbit
E_1	always	$\mathcal{H}'_1 = 3(\lambda - 1)$	linear parallel
E_2	always	$\mathcal{H}'_2 = -3(\lambda - 1)$	linear parallel
E_3, E_4	$\lambda > 3/4$	$\mathcal{H}'_{3,4} = (10\lambda^2 - 18\lambda + 9)/2\lambda$	elliptic
E_5, E_6	$\lambda > 3/8$	$\mathcal{H}'_{5,6} = (34\lambda^2 - 18\lambda + 9)/10\lambda$	linear

In the searching of the equilibria points, it is straightforward to arrive at the six following equilibria:

(i) In the interval $0 \leqslant \lambda \leqslant 1$, $E_{1,2} = (0, \pm 1, 0)$. The position of these equilibria is independent of λ.

(ii) In the interval $3/4 \leqslant \lambda \leqslant 1$,

$$E_{3,4} = (0, 3(\lambda - 1)/\lambda, \pm\sqrt{1 - 9(\lambda - 1)^2/\lambda^2}).$$

(iii) In the interval $3/8 \leqslant \lambda \leqslant 1$,

$$E_{5,6} = (3(\lambda - 1)/5\lambda, \pm\sqrt{1 - 9(\lambda - 1)^2/25\lambda^2}, 0).$$

In Table 1 are summarized the equilibria, their conditions of existence, the corresponding energy and the kind of orbit that they represent.

3.3. Stability of the equilibria

In order to determine the stability of the equilibria, we analyze the roots of the characteristic equation $\mathcal{A}$, resulting from the variational equations of motion

$$\begin{aligned}
\frac{\mathrm{d}}{\mathrm{d}\tau}\delta u &= -\lambda w\delta v + (3\lambda - 3 - \lambda v)\delta w,\\
\frac{\mathrm{d}}{\mathrm{d}\tau}\delta v &= -4\lambda w\delta u - 4\lambda u\delta w,\\
\frac{\mathrm{d}}{\mathrm{d}\tau}\delta w &= (3 - 3\lambda + 5\lambda v)\delta u + 5\lambda u\delta v,
\end{aligned} \tag{10}$$

which give rise to the characteristic equation $\mathcal{A}$,

$$\mathcal{A} = \kappa^3 + \kappa[9(1-\lambda)^2 + 20\lambda^2u^2 - 18(\lambda - 1)\lambda v + 5\lambda^2v^2 - 4\lambda^2w^2] + 8[9(\lambda - 1) - 5\lambda v]\lambda^2uw = 0. \tag{11}$$

For the equilibria $E_{1,2}$, $E_{3,4}$, $E_{5,6}$, the factor $uw = 0$, and the non-trivial part of Eq. (11) reduces to

$$\mathcal{A} = \kappa^2 + [9(1-\lambda)^2 + 20\lambda^2u^2 - 18(\lambda - 1)\lambda v + 5\lambda^2v^2 - 4\lambda^2w^2] = 0. \tag{12}$$

The root $\kappa = 0$ arises from the variational equation $u\delta u + v\delta v + w\delta w = 0$ [17].

By substituting in Eq. (12) the coordinates of the equilibria, we obtain the following characteristic equations as well as the following stability properties,

(i) E_1 is always stable because the roots of its characteristic polynomial

$$\kappa^2 + (9 - 4\lambda^2) = 0$$

are imaginary since $9 - 4\lambda^2 > 0$.

(ii) E_2 is stable when the two roots of its characteristic equation

$$\kappa^2 + (9 - 36\lambda + 32\lambda^2) = 0$$

are imaginary. That condition holds when

$$(9 - 36\lambda + 32\lambda^2) > 0 \Rightarrow \lambda \notin [3/8, 3/4].$$

In this way, E_2 is stable if $\lambda \in [0, 3/8) \cup (3/4, 1]$.

(iii) $E_{4,3}$ are stable when the two roots of the characteristic equation

$$\kappa^2 + (36 - 72\lambda + 32\lambda^2) = 0$$

are imaginary. That condition holds when

$$(36 - 72\lambda + 32\lambda^2) > 0 \Rightarrow \lambda \notin (3/4, 3/2).$$

Because $E_{3,4}$ only exist if $3/4 \leqslant \lambda \leqslant 1$, both equilibria are unstable.

(iv) $E_{5,6}$ are stable when the two roots of the characteristic equation

$$\kappa^2 + (-36 + 72\lambda + 64\lambda^2)/5 = 0$$

are imaginary. That condition holds when

$$(-36 + 72\lambda + 64\lambda^2) > 0 \Rightarrow \lambda \notin (-3/2, 3/8).$$

Because these equilibria only exist if $\lambda \geqslant 3/8$, they are always stable.

3.4. Parametric bifurcations and phase flow evolution

The previous stability analysis indicates the presence of the *parametric bifurcations* at the values $\lambda = 3/8$ and $\lambda = 3/4$. We can confirm the presence of bifurcations by studying the evolution, as a function of λ, of the energies at the equilibria (see Fig. 1). We observe in this figure that $\mathcal{H}'$ reaches its absolute minimum at the equilibrium E_1, and it does so on the whole interval $0 \leqslant \lambda \leqslant 1$. As a consequence of the Lyapunov theorem [18], this equilibrium is always stable. Over the interval $0 \leqslant \lambda \leqslant 3/8$ the absolute maximum is reached at the equilibrium E_2. Thus, by the Lyapunov theorem the equilibrium E_2 is also stable. When $\lambda = 3/8$ the equilibria $E_{5,6}$ appear. For $\lambda > 3/8$ the value of the energy at those points $\mathcal{H}'_{5,6}$ is a maximum and, for the same reason as before, they are stable. On the other hand, starting with this value of λ, the equilibrium E_2 changes its stability, becoming unstable. While λ stays below 3/4, this situation occurs. When $\lambda = 3/4$ the equilibria $E_{3,4}$ appear. While the equilibria $E_{5,6}$ and E_1 remain stable because their energies are maximum and minimum, respectively, the equilibrium E_2 changes again its stability, and the new $E_{3,4}$ are unstable. The diagram of Fig. 2 illustrates the described evolution of the equilibria stability, as well as indicating the kind of bifurcations that occur at $\lambda = 3/8$ and $\lambda = 3/4$.

A more detailed study of the behavior of the systems as a function of λ shows that it becomes detached from the phase flow evolution, which is shown in Fig. 3. When $\lambda < 3/8$ the phase flow consists of clockwise rotations around the stable equilibria $E_{1,2}$ (see Fig. 3a). Both equilibria correspond to linear parallel orbits to the external fields. The phase trajectories around the equilibria $E_{1,2}$ are vibrational levels, belonging to the Cacciani's class I.

When λ reaches the value 3/8 a *pitchfork* bifurcation [19] occurs: from E_2 (which becomes unstable) to the two stable equilibria $E_{5,6}$. The phase space structure changes. A homoclinic orbit (separatrix) that

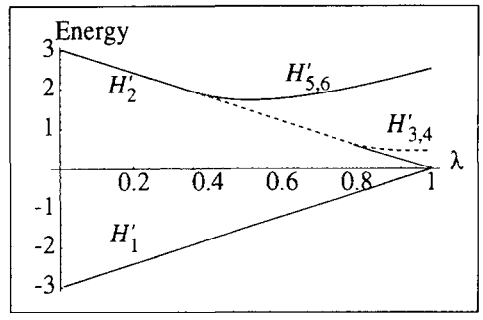

Fig. 1. Evolution of the values of the energy at the equilibria as a function of the parameter λ. Dashed lines indicate instability.

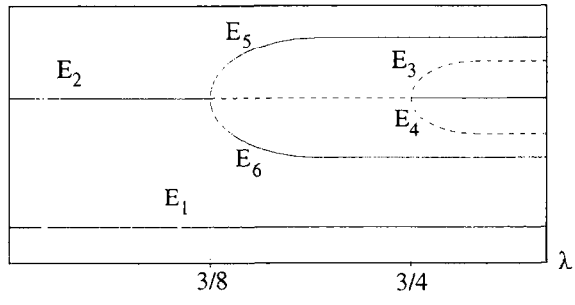

Fig. 2. Bifurcation diagram when the parameter λ varies from 0 to 1. Dashed lines indicate instability.

starts on E_2 and surrounds $E_{5,6}$ divides the phase space in two different zones of motion: one zone of rotations around E_1 and two zones of rotations around $E_{5,6}$ (see Figs. 3b,c). The new phase trajectories around $E_{5,6}$ correspond to the Cacciani's class III. The levels around $E_{1,2}$ still belong to vibrational motion. The new equilibria $E_{5,6}$ correspond to linear orbits which start parallel to the fields at $\lambda = 3/8$. As this parameter increases, these orbits gradually tend to be perpendicular to the fields. At the same time, the separatrix grows in such a way that the lobes surrounding $E_{5,6}$ are tangent in E_2 at $\lambda = 3/4$. Then, a second *pitchfork* bifurcation occurs. The equilibrium E_2 becomes stable again, and at the same time, emanating from it, two unstable equilibria $E_{3,4}$ appear. Now, two homoclinic orbits divide the phase space in three regions: one of rotations around E_1, one of rotations around E_2 and a third one around $E_{5,6}$ (see Figs. 3d,e). The new levels around E_2 form the Cacciani's class II. We note that the equilibria $E_{3,4}$ represent elliptic orbits, which are circular in the limit $\lambda = 1$. In this limit the values of the energies at the equilibria E_1 and E_2 coincide, and there arises the remarkable state of symmetry charac-

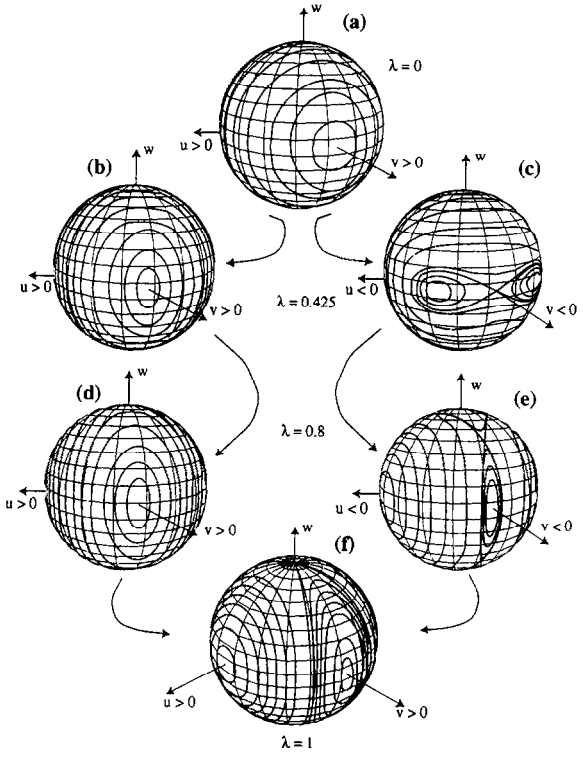

Fig. 3. Phase flow evolution as a function of the parameter λ.

teristic of the pure quadratic Zeeman effect, already described by Coffey et al. [11] (see Fig. 3f). Moreover, class levels I and II are both vibrational levels, while class levels III are rotational motion.

4. Poincaré surfaces of section

4.1. Scaling and regularization

As we saw in Section 2, the classical dynamics of the polar SQZE is described by the Hamiltonian (3). We can define a new reference frame in the *orbital plane* with coordinates (x, y), in such a way that the Hamiltonian (3) converts to

$$\mathcal{H} = \epsilon = \tfrac{1}{2}(P_x^2 + P_y^2) - \frac{1}{\sqrt{x^2+y^2}} + \tfrac{1}{8}\gamma^2 x^2 + fy. \tag{13}$$

In this orbital frame the y coordinate corresponds to the coordinate z, while the x coordinate corresponds to $\pm\rho$. Now, it is convenient to scale coordinates and momenta as [20] $\hat{\boldsymbol{r}} = \gamma^{2/3}\boldsymbol{r}$, $\hat{\boldsymbol{P}} = \gamma^{-1/3}\boldsymbol{P}$. After dropping hats, the Hamiltonian (13) becomes

$$\mathcal{H}\gamma^{-2/3} = \epsilon = \tfrac{1}{2}(P_x^2 + P_y^2) - \frac{1}{\sqrt{x^2+y^2}} + \tfrac{1}{8}x^2 + \mathcal{F}y, \tag{14}$$

and the classical dynamics depends only on the scaled energy $\epsilon = \gamma^{-2/3}E$ and the scaled electric field $\mathcal{F} = \gamma^{-4/3}f$, which represents the relative influence of the magnetic and the electric field strengths.

In order to avoid the numerical problems arising from the Coulomb singularity in the Hamiltonian (14) at $r \to 0$, we perform the so-called Levi–Civita regularization [21]. The first step of this procedure consists of a transformation to semiparabolic coordinates according to

$$\begin{aligned} x &= \frac{u^2 - v^2}{2}, \\ P_x &= u\frac{\mathrm{d}u}{\mathrm{d}t} - v\frac{\mathrm{d}v}{\mathrm{d}t} = up_u - vp_v, \\ y &= uv, \quad P_y = v\frac{\mathrm{d}u}{\mathrm{d}t} + u\frac{\mathrm{d}u}{\mathrm{d}t} = vp_u + up_v. \end{aligned} \tag{15}$$

Eq. (15) defines a transformation of coordinates which associates the axis $v = 0$ with $x > 0$ and the axis $u = 0$ with $x < 0$. In the new variables the Hamiltonian (14) is given by

$$\mathcal{H} = \tfrac{1}{2}(u^2+v^2)(p_u^2 + p_v^2) - \frac{2}{u^2+v^2} + \tfrac{1}{32}(u^2 - v^2)^2 + \mathcal{F}uv. \tag{16}$$

The next step is the definition of a new time $\tau = (1/2r)t$. Finally, the regularization is completed by multiplying the expression (16) by $u^2 + v^2$ and reorganizing in such a way that we obtain the pseudo-Hamiltonian

$$\mathcal{K} = 2 = \tfrac{1}{2}(P_u^2 + P_v^2) - \epsilon(u^2+v^2) + \tfrac{1}{32}(u^2+v^2)(u^2-v^2)^2 + \mathcal{F}uv(u^2+v^2), \tag{17}$$

where $P_u = \mathrm{d}u/\mathrm{d}\tau$ and $P_v = \mathrm{d}v/\mathrm{d}\tau$. We observe that, for negative scaled energies ϵ (bounded orbits), the Hamiltonian (17) describes a two-dimensional isotropic harmonic oscillator of frequency $\sqrt{-2\epsilon}$, coupled by means of two polynomials of sixth and fourth order, which represent, respectively, the magnetic and

the electrical field strengths. Now, the Hamiltonian (17) presents the most convenient form for numerical investigations.

4.2. Poincaré surfaces of section

We use the technique of Poincaré surfaces of section to describe the classical electronic structure of the SQZE polar: By keeping ϵ constant and by tuning the parameter $\mathcal{F}$, we explore the structure of the surfaces of section (SOS) as the system evolves from pure Zeeman effect to Stark effect. The structure of an SOS is determined by the number and stability of the fixed points (periodic orbits) appearing in the SOS. In accordance with the previous classical perturbation study, we show that the behavior observed in the Poincaré surfaces, coincides, qualitatively, with the predicted behavior by perturbation methods.

Following Friedrich and Wintgen [20], we define the surface of section as $u = 0$ and $P_u > 0$. Under these conditions, the SOS is bounded by the condition $P_v = \pm(4 + 2\epsilon v^2 - \frac{1}{16}v^6)^{1/2}$. It is worth noting that, when $\mathcal{F} = 0$, the limit of the surface of section corresponds to the equatorial linear periodic orbits (y and P_y permanently equal zero).

To begin with the study, we fix a constant energy $\epsilon = -1$ because for a wide range of values of $\mathcal{F}$, classical orbits are bounded, i.e., the energy value remains below the Stark saddle point energy [22]. Furthermore, for this energy value the behavior of the polar quadratic Zeeman system is very close to its integrable limit [20], and therefore presents regular behavior.

4.3. Evolution of the Poincaré surfaces of section

The evolution of the surfaces of section as well as the corresponding periodic orbits for $\mathcal{F}$ varying from 0 to 0.2 is shown in Fig. 4. The sequence begins with the pure Zeeman effect ($\mathcal{F} = 0$, Fig. 4a). This figure shows three important structures.

(i) The stable (elliptic) fixed point located at (0,0) which corresponds to an equatorial linear orbit perpendicular to the fields with $x \geqslant 0$. The symmetric linear periodic orbit perpendicular to the fields with $x \leqslant 0$ corresponds, as we noted, to the limit of the surface of section. Following Wintgen [23] and Friedrich and Wintgen [20], we label these orbits as I_1 and I_1'. The levels around I_1 belong to the quasi-periodic rotational motion.

(ii) The elliptic fixed points in $(0, \pm\sqrt{2})$ are, respectively, linear periodic orbits parallel to $y \geqslant 0$ (labeled as I_∞) and parallel to $y \leqslant 0$ (labeled as I_∞') to the fields. The levels around I_∞ and I_∞' correspond to the quasi-periodic vibrational motion.

(iii) The two hyperbolic (unstable) fixed points of the separatrix divide the previous two regions of motion. These points correspond to elliptic periodic orbits which, when $\epsilon \to \infty$, are circular orbits located at $(\pm 1, 0)$. These circular periodic orbits and the hyperbolic equilibria are both labeled as C.

When the electric field is turned on (see Fig. 4b), the symmetry of the vibrational states is broken: The hyperbolic points migrate towards the elliptic I_∞, while the elliptic equilibrium I_1 moves along the axis $P_v > 0$. The elliptic points $I_{\pm\infty}$ stay static. As a consequence, the periodic orbit I_1 is not already perpendicular to the fields, and the periodic orbits C and C' become elliptic. Now, the limit of the surface of section when $\mathcal{F} \neq 0$ does not correspond to any periodic orbit, and then the periodic orbit I_1' is compelled to evolve to a new periodic orbit located, as a fixed point, inside the surface of section. However, this periodic orbit is not at a glance observable. To detect this point, we have enlarged the mentioned zone of the surface of section in Fig. 4b, where we observe the presence of a new fixed point, which corresponds to the symmetric linear orbit to I_1. We label again this periodic orbit as I_1'. The appearance of this new periodic orbit is not associated with any kind of bifurcation because, when the surface of section is defined on a finite and closed space, orbits can appear and disappear at the boundary [24].

As the parameter $\mathcal{F}$ increases, the described trend continues (see Fig. 4c). Finally, when the Stark parameter reached the value $\mathcal{F} = 0.05$, the collapse between these equilibria occurred: The equilibria C have disappeared (see Fig. 4d), while the surviving equilibrium I_∞ becomes unstable. A *pitchfork* bifurcation occurs.

When the Stark parameter increases ($\mathcal{F} = 0.09$, 0.13, 0.16), the equilibria I_1 and I_1' are still simultaneously moving along the axis $P_v > 0$ towards the equilibrium I_∞ (see Figs. 4e,f,g). As we can observe in these figures, the fixed point I_1' is already visible in the surfaces of section. When $\mathcal{F} = 0.2$ (see Fig. 4h),

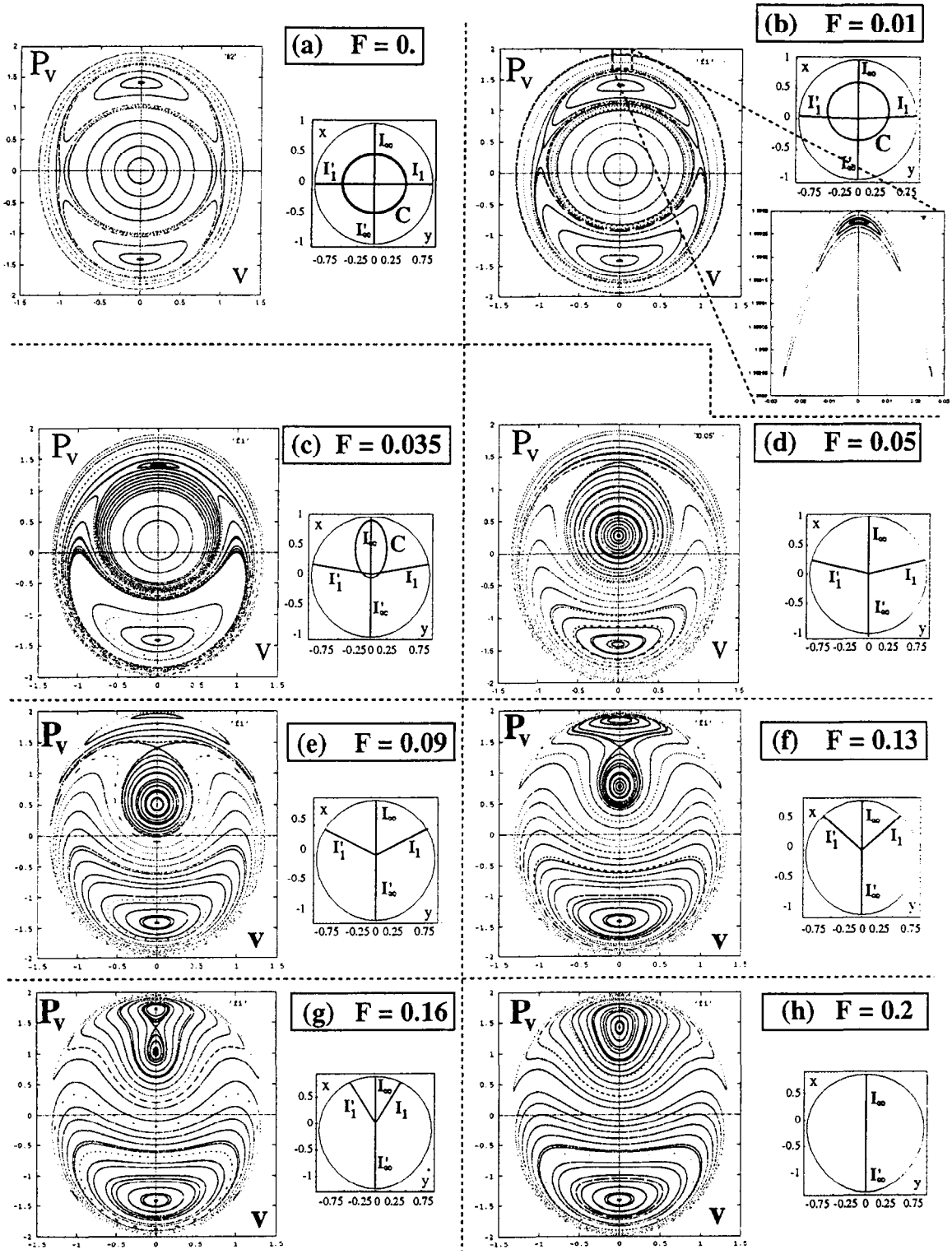

Fig. 4. Evolution of the Poincaré surfaces of section as a function of the parameter $\mathcal{F}$.

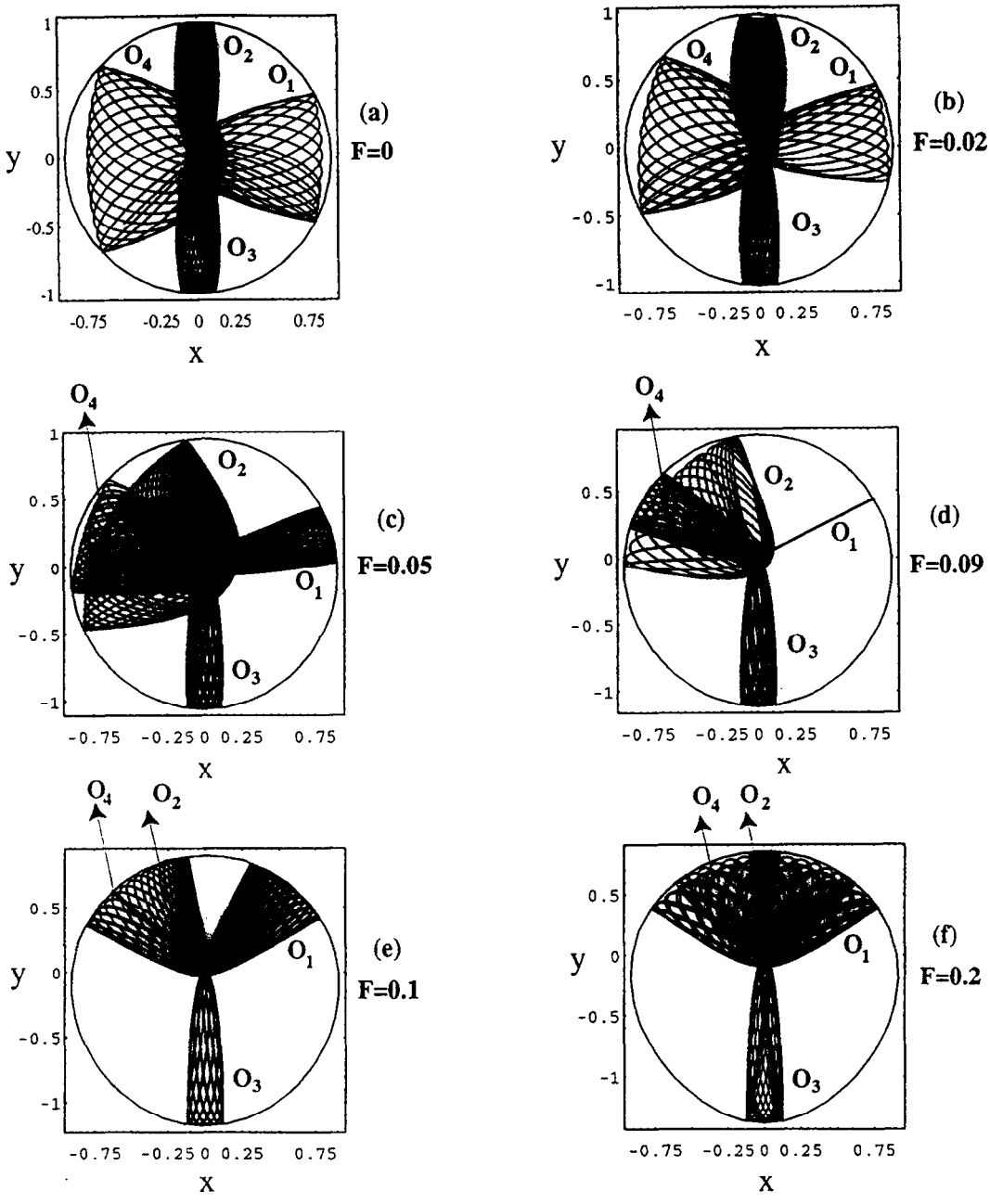

Fig. 5. Evolution of the quasi-periodic levels as a function of the parameter $\mathcal{F}$.

these three equilibria come into coincidence in such a way that only I_∞ survives, also becoming stable. In this way, a second *pitchfork* bifurcation occurs. After the bifurcation, the levels around the stable equilibria I_∞ and I'_∞ both belong to vibrational motion, which indicates that the Stark regime is reached. These two classes of vibrational motion are kept apart by means of a special separatrix that contains no fixed point: Both classes of vibrational motion evolve in a smooth way from one class to another [1].

4.4. Evolution of the level structure

Once the evolution of the periodic orbits (fixed points) has been stated, it is convenient to study the evolution of the levels around these fixed points (quasi-periodic orbits), because this provides insights into both quantum calculations and experimental results. To begin with, we take four quasi-periodic orbits named as O_1, O_2, and O_3 and O_4, of which the initial conditions, when $\mathcal{F} = 0$, are located, respectively, in each of the four different zones of motion of the surface of section in Fig. 4a. The evolution of these four quasi-periodic orbits is shown in Fig. 5. When $\mathcal{F} = 0$, O_1 and O_4 are rotational levels, while O_2 and O_3 are vibrational levels (Fig. 5a). From the point of view of quantum mechanics, we may associate the vibrational levels O_2 and O_3 with the twofold degenerate states of opposite parity, of which the wave functions are stretched along the direction of the magnetic field: the so-called Cacciani's levels of class I (O_2) and II (O_3). On the other hand, the rotational levels O_1 and O_4 may be associated with quantum states of which the wave functions are located in the plane $z = 0$: Cacciani's levels of class III.

When $\mathcal{F}$ is turned on, we observe that O_3 stays as vibrational level for all values of $\mathcal{F}$ because the periodic orbit I_∞ is not involved in any bifurcation. However, the remaining quasi-periodic orbits O_1, O_2 and O_4 are affected for the bifurcations and they evolve in the same way as the different zones of motion in the surface of section evolve.

As $\mathcal{F}$ increases, the primitive rotational levels O_1 and O_4 are becoming vibrational. In this way, when the first bifurcation has not occurred, both levels evolve as the periodic orbits I_1 and I_1' do (see Figs. 5b,c). On the other hand, O_2 remains vibrational until the first bifurcation occurs. After this bifurcation occurs, O_2 suddenly loses its vibrational character, acquiring the same nature as O_4 (Fig. 5c). From the point of view of Cacciani's classes, this behavior corresponds to a mixing regime of states belonging to the classes I and III.

After the first bifurcation, as the electric field grows, the evolution of the O_1, O_2 and O_4 is determined for the evolution of periodic orbits I_1 and I_1' in such a way that, circumstantially, they come into coincidence (see Figs. 5d,e). Finally, when the second bifurcations occurs, we observe in Fig. 5f that the quasi-periodic orbits O_1, O_2 and O_4 belong to the vibrational motion. That is to say, the Stark regime is reached, and only vibrational states are present (Cacciani's classes I and II).

5. Conclusions

We have shown that the transition from Zeeman effect to Stark effect is produced via two pitchfork bifurcations. Moreover, it is possible to state a remarkable analogy between the phase space structure found by means of surfaces of section and the phase portrait of the normalized Hamiltonian. Finally, we find that these classical treatments are able to explain the Stark structure of the hydrogenic diamagnetic structure detected in experimental and semiclassical studies of the lithium atom.

Acknowledgement

This research was partially supported by the project PB 95-0795 of the Ministerio de Educación y Cultura of Spain.

References

[1] R.L. Waterland, J.B. Delos, M.L. Du, Phys. Rev. A 35 (1987) 5064.
[2] P. Cacciani, S. Liberman, E. Luc-Koenig, J. Pinard, C. Thomas, J. Phys. B 21 (1988a) 3473.
[3] P. Cacciani, S. Liberman, E. Luc-Koenig, J. Pinard, C. Thomas, J. Phys. B 21 (1988b) 3499.
[4] P. Cacciani, S. Liberman, E. Luc-Koenig, J. Pinard, C. Thomas, J. Phys. B 21 (1988c) 3523.
[5] D. Farrelly, T. Uzer, P.E. Raines, J.P. Skelton, J.A. Milligan, Phys. Rev. A 45 (1992) 4738.
[6] A. Deprit, V. Lanchares, M. Iñarrea, J.P. Salas, J.D. Sierra, Phys. Rev. A 54 (1996) 3885.
[7] J. von Milczewski, T. Uzer, Phys. Rev. A 56 (1997) 220.
[8] H.J. Poincaré, Les Méthodes Nouvelles de la Mécanique Céleste 1, Ch. 3 (Gauthier-Villars, Paris, 1982).
[9] P.A. Braun, E.A. Solov'ev, Sov. Phys. JETP 59 (1984) 38.
[10] P.A. Braun, Rev. Mod. Phys. 65 (1993) 115.
[11] S.L. Coffey, A. Deprit, B.R. Miller, C.A. Williams, Ann. New York Acad. Sci. 497 (1986) 22.
[12] J.B. Delos, S.K. Knudson, D.W. Noid, Phys. Rev. A 28 (1983) 7.
[13] B. Goldstein, Classical Mechanics, 2nd ed. (Addison-Wesley, Reading, MA, 1980).
[14] A. Deprit, Celest. Mech. 26 (1981) 9.

[15] S. Wolfram, Mathematica, a System for Doing Mathematics by Computer (Addison Wesley, New York, 1990).
[16] A. Deprit, S. Ferrer, Rev. Acad. Ciencias Zaragoza 45 (1990) 111.
[17] J.E. Marsden, T.S. Ratiu, Introduction to Mechanics and Symmetry, Text in Appl. Mathematics 17 (Springer, New York, 1994).
[18] E.A. Coddington, N. Levinson, Theory of Ordinary Differential Equations (McGraw Hill, New York, 1995).
[19] P. Glendinning, Stability, Unstability and Chaos, Cambridge Text in Appl. Mathematics (1994).
[20] H. Friedrich, D. Witntgen, Phys. Rep. 183 (1989) 37.
[21] T. Levi-Civita, Sur la Resolution Qualitative du Porbléme des trois Corps, University of Bologna, Vol. 2 (1956).
[22] D. Farrelly, J.E. Howard, Phys. Rev. A 49 (1994) 1494.
[23] D. Wintgen, J. Phys. B 20 (1987) L511.
[24] J.M. Mao, J.B. Delos, Phys. Rev. A 45 (1992) 1746.